Author(s): Lehtovaara, Lauri & Havu, Ville & Puska, Martti J.

Title: All-electron time-dependent density functional theory with finite elements: Time-propagation approach

Year: 2011

Version: Final published version

Please cite the original version:

Lehtovaara, Lauri & Havu, Ville & Puska, Martti J. 2011. All-electron time-dependent density functional theory with finite elements: Time-propagation approach. The Journal of Chemical Physics. Volume 135, Issue 15. 154104/1-8. ISSN 1089-7690 (electronic). DOI: 10.1063/1.3651239.

All-electron time-dependent density functional theory with finite elements: Time-propagation approach

Lauri Lehtovaara, Ville Havu, and Martti Puska

Citation: The Journal of Chemical Physics **135**, 154104 (2011); doi: 10.1063/1.3651239
View online: http://dx.doi.org/10.1063/1.3651239
View Table of Contents: http://scitation.aip.org/content/aip/journal/jcp/135/15?ver=pdfcov
Published by the AIP Publishing

All-electron time-dependent density functional theory with finite elements: Time-propagation approach

Lauri Lehtovaara,[1,2,a)] Ville Havu,[1] and Martti Puska[1]
[1]*Department of Applied Physics, Aalto University, P.O. Box 11100, FI-00076 Aalto, Finland*
[2]*LPMCN, Université Claude Bernard Lyon I and CNRS, 69622 Villeurbanne, France*

(Received 10 June 2011; accepted 23 September 2011; published online 17 October 2011)

We present an all-electron method for time-dependent density functional theory which employs hierarchical nonuniform finite-element bases and the time-propagation approach. The method is capable of treating linear and nonlinear response of valence and core electrons to an external field. We also introduce (i) a preconditioner for the propagation equation, (ii) a stable way to implement absorbing boundary conditions, and (iii) a new kind of absorbing boundary condition inspired by perfectly matched layers. © *2011 American Institute of Physics*. [doi:10.1063/1.3651239]

I. INTRODUCTION

The introduction of attosecond lasers has provided experimental access to electron dynamics.[1] Attosecond pulses have a time span of the same order as classical periods of electrons on valence shells. Therefore, they can be used to take "snapshots" of electron dynamics. For example, in a recent experiment, the motion of valence electrons was recorded in real-time.[2] A krypton atom was excited (pumped) by a high intensity near-infrared (NIR) femtosecond laser pulse and then probed by following extreme-ultraviolet (EUV) attosecond laser pulses with different delays with respect to the NIR pulse. Modelling such an experiment theoretically poses several difficulties. The high intensity of the NIR pulse causes nonlinear effects and therefore perturbative approaches become questionable. The EUV pulse has an average energy of ~80 eV and the short duration of the pulse ($\leq$150 as) implies a broad energy range. Therefore, not only the valence electrons are excited (or ionized), but actually the measurement process itself relies on the excitation of a core electron to a hole in valence states. Even though the experiment was performed with krypton atoms, the systems of interest are not only atoms or simple molecules, but for example, complex biological systems and surfaces with adsorbed molecules. Therefore, it is crucial to develop theoretical and computational methods which are able to treat the dynamics of both the bond-forming valence as well as that of the rather inert core electrons beyond the linear response regime.

The density functional theory (DFT) is widely used in the electronic structure theory of materials, surfaces, and molecules.[3] Its success derives from its ability to provide accurate results with a reasonable computational effort. However, DFT is bound to static systems. While some recent advances in DFT, such as hybrid exchange-correlation (XC) functionals, are capable of reproducing some excited state properties (e.g., band gaps) relatively well, DFT cannot describe the dynamics of electrons on excited states. The time-dependent DFT (TDDFT) is based on the Runge-Gross theorem[4] which states that any two (physically) different time-dependent external potentials (e.g., laser fields) give disparate time evolutions of the electron density. The theorem extends DFT to excited states and to the dynamics of electrons under time-dependent external fields in a justified way.

The time-propagation (TP) approach to TDDFT,[5] where time-dependent Kohn-Sham (TDKS) equations are propagated in real-time (in contrast to solving them in frequency space), allows modelling of laser pulses of any frequency, shape, and intensity.[6] The nonlinear effects can be modelled without any changes to the underlying equations and the only theoretical limiting factor is the quality of the approximated XC functional. The current XC functionals for TDDFT are known not to perform well in all cases, but they perform adequately in many cases and are under active development.[7,8]

The time-propagation approach has also advantages from the numerical point of view, which makes it suitable for large systems. The computational cost scales well with respect to increasing system size,[9] and it allows efficient parallelization over TDKS states.

When modelling electron dynamics, especially in the nonlinear response limit (e.g., harmonic generation), absorbing boundary conditions[10,11] decrease unwanted scattering from the boundaries of the simulation cell significantly, and therefore, reduce artificial boundary effects. Mainly two approaches have been used with TDDFT: the negative imaginary potential and the mask function.[12] These methods are simple to implement and they can be tuned to absorb one frequency efficiently. However, their performance begins to deteriorate as a wider range of frequencies reach the boundary. The perfectly matched layers (PMLs) method[13] is an absorbing boundary which adapts to the incoming wave. It is widely used, for example, in field of electromagnetic scattering. It has also been applied to Schrödinger equation,[14] but the equations become tedious and the propagation matrix is no longer complex symmetric, which slows down the numerical solution process.

The computer implementation of TP-TDDFT formalism requires a discretization scheme, for example, planewaves,[15]

a)Electronic mail: lauri.lehtovaara@iki.fi.

real-space grid,[12,16] or atomic orbital basis.[17] Desirable properties for a TP-TDDFT discretization scheme include (i) accuracy which is insensitive to external field, (ii) systematically improvable accuracy, (iii) efficient use of degrees of freedom (DOF), and (iv) efficient parallelization. Atomic orbital bases are fast and efficient for the ground state of a system, but their performance begins to deteriorate when the system evolves far from the ground state. Increasing the degrees of freedom does not necessarily increase the accuracy in a systematic way. With planewaves and finite-difference (FD) discretization (i.e., uniform real-space grids), the inherent accuracies for the ground and excited states do not significantly differ, and by increasing the degrees of freedom, accuracy increases systematically. However, in practice, planewaves and FD scheme require pseudo-potentials[18] (or similar approaches, such as the projector-augmented wave (PAW) method[19]) in order to avoid sharp wave function oscillations and large electron density gradients near nuclei. This leads to additional error, which is not straightforward to estimate and control. Moreover, an artificial division to "core" and "valence" states must be made, which sets limits for accuracy. In most systems, the choice of "core" states is clear, but still in many other system it is not clear beforehand, especially in the time-dependent case. A single "semi-core" state might require a much denser discretization than that required by other states contributing to the phenomenon under study. As a consequence, efficiency drops because of significant overdiscretization. Also large vacuum regions inside simulation cells are inefficiently handled by uniform discretizations.

The finite element (FE) discretization[20,21] can be used for nonuniform discretization of the real-space. It is a linear combination of continuous, piecewise polynomial functions. It inherits the good properties of the real-space methods, such as, flexible boundary conditions and efficient parallelization via domain decomposition, while still allowing a nonuniform discretization. As finite elements can adapt to the local feature size, they can be used to describe solutions of core and valence electrons equally well. Moreover, they can adapt to the geometry of the system to avoid overdiscretization. We have described our FE discretization in our previous paper.[22] The FE mesh is created by merging highly nonuniform but symmetric atomic meshes to a global, nonuniform, and unstructured mesh.

There exists a few earlier attempts to apply the FE methodology to time-dependent electronic structure calculations.[23–26] However, none of these uses hierarchical elements on unstructured meshes. Moreover, these are either single particle calculations or Hartree-Fock calculations for a few electrons, not TDDFT calculations for tens of electrons.

The rest of the paper is structured as follows. In the next section, we briefly review TDDFT, TP-TDDFT, and the FE method. In Sec. III, we present a preconditioner for TP-TDDFT, discuss propagation with absorbing boundary conditions, and describe a PML like boundary condition. In Sec. IV, we apply our implementation to a set of well known systems in the linear response regime, namely, sodium dimer Na_2, benzene C_6H_6, and fullerene C_{60} molecules. For Na_2, we calculate semi-core excitations in addition to valence excitations. Furthermore, we apply an intense laser pulse to a Mg atom in order to test the nonlinear regime. Finally, we probe the valence electrons of a Mg atom by semi-core excitations before and after an intense laser pulse. In the final section, we draw the conclusions and set directions for future research.

We will use the atomic units throughout the article.

II. THEORY

A. Time-dependent density functional theory

In the TDDFT, no variational principle exists, but the quantum mechanical action

$$A[\psi] = \int_{t_0}^{t_1} dt \langle \psi(t) | i \frac{\partial}{\partial t} - \hat{H}(t) | \psi(t) \rangle, \tag{1}$$

defined by the time-dependent Hamiltonian $\hat{H}(t)$ of the system, provides an analogous quantity to the total energy of the ground-state DFT.[27] The TDKS equation reads

$$\begin{aligned} i \frac{\partial}{\partial t} \psi_k(\mathbf{r}, t) &= \hat{H}_{\mathrm{KS}}[n](\mathbf{r}, t) \psi_k(\mathbf{r}, t) \\ &= \left(-\frac{1}{2} \nabla^2 + v_{\mathrm{KS}}[n](\mathbf{r}, t) \right) \psi_k(\mathbf{r}, t), \end{aligned} \tag{2}$$

where $\psi_k(\mathbf{r}, t)$ are the TDKS orbitals and $v_{\mathrm{KS}}[n](\mathbf{r}, t)$ is the effective TDKS potential. The TDKS orbitals ψ_k are orthonormal $\langle \psi_i | \psi_j \rangle = \delta_{ij}$ and provide the time-dependent density $n(\mathbf{r}, t) = \sum_k f_k |\psi_k(\mathbf{r}, t)|^2$, where f_k is the occupation of k^{th} state. The density is normalized to the total number of electrons $N_{el} = \int n(\mathbf{r}, t) d^3 r$ in the system.

The time-dependent effective potential $v_{\mathrm{KS}}[n](\mathbf{r}, t)$ reads as

$$v_{\mathrm{KS}}(\mathbf{r}, t) = v_H[n](\mathbf{r}, t) + v_{\mathrm{xc}}[n](\mathbf{r}, t) + v_{ext}(\mathbf{r}, t), \tag{3}$$

where $v_H[n](\mathbf{r}, t)$ is the Hartree potential, $v_{ext}(\mathbf{r}, t)$ is the external potential, and $v_{\mathrm{xc}}[n](\mathbf{r}, t)$ is the XC potential. The Hartree potential reads as

$$v_H[n](\mathbf{r}, t) = \int d^3 r' \frac{n(\mathbf{r}', t)}{|\mathbf{r} - \mathbf{r}'|}. \tag{4}$$

The external potential includes the electron-nucleus attraction $v_{ne}(\mathbf{r}, R_a, t)$ and a possible external field (e.g., a laser field) $v_{field}(\mathbf{r}, t)$. The electron-nucleus attraction

$$v_{ne}(\mathbf{r}) = \sum_{a=1}^{N_{nuc}} \frac{-Z_a}{|\mathbf{r} - \vec{R}_a|}, \tag{5}$$

depends on the nuclear positions $\vec{R}_a$ and nuclear charges Z_a. N_{nuc} is the number of nuclei in the system. The external field $v_{field}(\mathbf{r}, t)$ can be, for example, a simple monochromatic laser pulse within the dipole approximation

$$v_{pulse}(\mathbf{r}, t) = -(\vec{E}_0 \cdot \vec{r}) g(t) \sin(\omega t), \tag{6}$$

where $\vec{E}_0$ gives the strength and polarization direction of the electric field and $g(t)$ is an envelope function, which should be chosen so that the total pulse area is zero.[28,29]

The true time-dependent exchange-correlation potential $v_{\mathrm{xc}}[n](\vec{r}, t)$ is nonlocal in space and it depends on all previous densities, i.e., it has memory. However, it is unknown and

must be approximated. In this work, we apply the adiabatic local density approximation (ALDA),[30] which is local both in space and in time.

B. Finite elements

The present FE discretization scheme and mesh generation approach have been described in detail in our earlier paper.[22] Thus, we only briefly review the FE method here.

The FE method divides a computation domain into polyhedra, for example, tetrahedra which are used in our implementation. Inside each polyhedron, a set of polynomials forms a local basis. This basis can be chosen hierarchically in which case a higher order basis includes all the lower order bases. In a conforming method the global basis is then constructed by forcing continuity of the basis functions over vertices, edges, and faces of polyhedra. Still, the global basis functions remain local and span only elements sharing a face, an edge, or a vertex. The resulting basis is a variational, hierarchical, local, continuous, and piecewise polynomial basis, which can be used for nonuniform discretization.

Our mesh generation scheme (for details, see Ref. 22) first constructs symmetric atomic meshes by adding spherical layers of vertices with exponentially increasing layer radius. The vertices of each layer are vertices of highly symmetric polyhedra. The symmetric atomic meshes are then merged together by a Delaunay tetrahedralization[31] and finally refined by a Delaunay refinement.[32] Our choice for a local basis is a hierarchical basis, where local basis functions are generated using products of one-dimensional integrated Legendre polynomials over the interval $[-1, 1]$.[33]

Once the global basis functions $\chi_k(\mathbf{r})$ are available, the KS states can be written as a linear combination

$$\psi_k(\mathbf{r}, t) = \sum_j C_{k,j}(t)|\chi_j(\mathbf{r})\rangle. \tag{7}$$

By substituting this into the TDKS Eq. (2), multiplying from left by $\langle\chi_i(\mathbf{r})|$, and integrating over the space we obtain the matrix equation

$$iS\frac{\partial}{\partial t}C(t) = H_{\mathrm{KS}}(t)C(t), \tag{8}$$

where the overlap matrix is

$$S_{ij} = \langle\chi_i|\chi_j\rangle, \tag{9}$$

and the Hamilton matrix is

$$H_{ij}^{\mathrm{KS}} = \frac{1}{2}\langle\nabla\chi_i|\nabla\chi_j\rangle + \langle\chi_i|v_{\mathrm{KS}}[n](\mathbf{r}, t)|\chi_j\rangle. \tag{10}$$

C. Time propagation

The TDKS equation is an initial value problem and can be solved using the TP scheme.[5] The partial differential equation (Eq. (2)) can be solved formally

$$\begin{aligned}\psi_k(\mathbf{r}, t) &= \hat{U}(t, t_0)\psi_k(\mathbf{r}, t_0)\\ &= \hat{\mathcal{T}}\exp\left[-i\int_{t_0}^{t}\hat{H}_{\mathrm{KS}}[n](\mathbf{r}, t')dt'\right]\psi_k(\mathbf{r}, t_0),\end{aligned} \tag{11}$$

where $\hat{U}(t_1, t_0)$ is the time-propagation operator and $\hat{\mathcal{T}}$ is the time-ordering operator. In practice, it is impossible to solve the above equation exactly for any physically relevant system. However, the total propagator $\hat{U}(t_1, t_0)$ can be rewritten as a product of propagators over short time intervals Δt, i.e.

$$\hat{U}(T, 0) = \Pi_{p=0}^{N_t-1}\hat{U}(t_p + \Delta t, t_p), \tag{12}$$

where $N_t = T/\Delta t$, and T is the total propagation time. In the limit of a short time-step, $\Delta t \to 0$, several approximations for the propagator $\hat{U}(t_p + \Delta t, t_p)$ can be found.[34]

The FE basis is not an orthonormal basis, which restricts the choice of the propagator in practice. In the FE discretized form, the original propagation Eq. (11) reads

$$C_k(\mathbf{r}, t) = \hat{\mathcal{T}}\exp\left[-i\int_{t_0}^{t}S^{-1}(t')H_{\mathrm{KS}}[n](\mathbf{r}, t')dt'\right]C_k(\mathbf{r}, t_0), \tag{13}$$

in which the inverse of the overlap matrix occurs inside the integral. Many of the propagators suitable for orthogonal bases would require the inverse $S^{-1}(t)$ to be calculated, which is prohibitively expensive for the FE basis. However, the well-known Crank-Nicolson (CN) method, which is also known as the implicit mid-point rule,[35]

$$\begin{aligned}\hat{U}_{\mathrm{CN}}(t + \Delta t, t) = &\left[\hat{1} + \frac{i}{2}\Delta t\hat{H}(t + \Delta t/2)\right]^{-1}\\ &\times\left[\hat{1} - \frac{i}{2}\Delta t\hat{H}(t + \Delta t/2)\right],\end{aligned} \tag{14}$$

is suitable for nonorthogonal bases.[36] Instead of actually calculating the inverse, the propagation equation can be cast into a set of matrix equations

$$\begin{aligned}&\left[S(t + \Delta t/2) + \frac{i}{2}\Delta t H_{\mathrm{KS}}(t + \Delta t/2)\right]C(t + \Delta t)\\ &= \left[S(t + \Delta t/2) - \frac{i}{2}\Delta t H_{\mathrm{KS}}(t + \Delta t/2)\right]C(t)\\ &\quad + \mathcal{O}(\Delta t^3).\end{aligned} \tag{15}$$

The Hamilton matrix at the middle of the time-interval $H_{\mathrm{KS}}(t + \Delta t/2)$ is unknown beforehand, but it can be approximated by taking the average of the Hamiltonian at the beginning and at the end of the time-interval and using a self-consistent cycle (i.e., fixed point iteration) to solve the equation. In practice, instead of a full self-consistent cycle, it is sufficient to do only a single predict and a single correct step in order to achieve the third-order local convergence. The third-order local convergence provides the second-order global convergence, i.e., the error after the whole propagation, $t = T$, converges as $\mathcal{O}(\Delta t^2)$. We call the Crank-Nicolson propagator with one predict-correct step as the semi-implicit Crank-Nicolson (SICN).

1. Optical spectra

The optical absorption spectrum can be obtained from TP-TDDFT by first applying a weak delta pulse

$$E(t) = \vec{K}_0 \delta(t), \tag{16}$$

at time $t = 0$ to the system. The pulse excites all possible frequencies with equal intensity, i.e.

$$\psi_k(t = 0^+) = \exp\left[i \int_{t=0^-}^{0^+} \vec{K}_0 \cdot \mathbf{r} \delta(t) dt \right] \psi_k(t = 0^-)$$
$$= \exp[i \vec{K}_0 \cdot \mathbf{r}] \psi_k(t = 0^-), \tag{17}$$

and then the system is let to evolve freely in time. The time-evolution of the time-dependent dipole moment (TDDM)

$$\vec{\mu}(t) = -\langle \psi_k(t) | \vec{r} | \psi_k(t) \rangle, \tag{18}$$

is recorded. Then the Fourier transform of the TDDM gives the optical absorption spectrum[37] (parallel to electric field)

$$S_\parallel(\omega) = \frac{2\omega}{\pi} \frac{1}{|\vec{K}_0|} \int_0^T (\mu_\parallel(t) - \mu_\parallel(0^-)) \sin(\omega t) g(t) dt, \tag{19}$$

where ω is the excitation energy, and $g(t)$ is an envelope function (e.g., Gaussian).

TP-TDDFT is also capable of handling nonlinear phenomena. The nonlinear response of a system to a continuous-wave (CW) laser field with frequency ω_f causes optical emission spectrum to include higher harmonics, i.e., integer multiples of the field frequency ω_f[38]. The nonlinear optical emission spectrum is proportional to the power spectrum of the acceleration of TDDM,[38,39]

$$H_\parallel(\omega) \propto \left| \omega^2 \int_0^T (\mu_\parallel(t) - \mu_\parallel(0^-)) \exp(-i\omega t) g(t) dt \right|^2. \tag{20}$$

III. TIME-PROPAGATION AND FINITE-ELEMENT BASIS

In this section, we will address specific issues by applying the time-propagation approach together with all-electron FE basis. The most essential part of a practical FE-TP method is the preconditioning of the propagation equation, which will be discussed next.

A. Preconditioning

The propagation matrix in Eq. (15) is relatively ill-conditioned on an all-electron FE basis as small elements near nuclei allow large kinetic energy values whereas large simulation cells allow very low kinetic energy values. Iterative methods, like conjugate gradient, applied to ill-conditioned systems converge slowly. However, the conditioning and thereby the convergence rate can be improved by preconditioning. If we write the propagation equation in the form

$$(\gamma S + H) C(t + \Delta t) = (\gamma S - H) C(t), \tag{21}$$

where $\gamma = -2i/\delta t$, it is fairly intuitive to choose an approximation of $(\alpha S + T)^{-1}$ as the preconditioner. The kinetic energy operator T compresses the high-energy end of the spectrum towards unity, whereas the shift αS prevents too aggressive smoothing in the low-energy end. Deeply bound core states are not an issue here, as those are few and well separated from the rest of the eigenvalue spectrum. Instead of using γ as shift, α is chosen to be a positive real number. With this choice, the preconditioner is symmetric positive definite, which is a desirable property from the numerical point of view. We have not yet tried to found a systematic way to chose the optimal value for α. However, according to our tests α should have the same order of magnitude as the excitation energy range of interest, i.e., it should be proportional to the inverse of the time-step.

The preconditioner $(\alpha S + T)^{-1}$ is approximated by a multilevel scheme, which first applies a multi-p scheme continued by the algebraic multigrid (AMG) scheme[40] for linear elements (p refers here to the polynomial degree of basis functions). The preconditioning cycle begins with weighted Jacobi relaxation sweeps with the weight of 0.25 for the whole system. Then the projection to the $(p - 1)$th level is made, i.e., the basis functions of the order p are excluded, and the Jacobi relaxation is repeated. These projection-relaxation steps are made until all basis functions are linear ($p = 1$). From this point onward, we continue with the AMG method,[40] which is known to work well with linear basis functions and the shifted Laplacian operator $(\alpha S + T)$. We use the smoothed aggregation AMG[41] implementation of the Trilinos library.[42,43]

B. Absorbing boundary conditions

In simulations where excitations occur to continuum states, the boundaries of a simulation cell must be treated properly. At the boundary of a simulation cell, a boundary condition (BC) must be chosen. For example, wave functions can be chosen to be zero at the boundary (Dirichlet BC), their derivative can be chosen to be zero (Neumann BC), or a periodic boundary condition can be applied. If the boundary is set to lie infinitely far from a system, all the three above boundary conditions are equal and do not cause any artificial boundary effects. However, an infinitely large simulation cell is computationally clearly unfeasible. On the other hand, without proper treatment a finite simulation cell causes artificial boundary effects, e.g., reflections and confinement effects.

Absorbing boundary conditions (ABC) try to mimic an infinitely large simulation cell (or open boundary) by trying to absorb all the outgoing electrons, which would never return to the simulation cell in the real system. In practice, ABC cannot differentiate between outgoing electrons which would return and which would not return. Nevertheless, a well-chosen ABC can significantly reduce unwanted artificial boundary effects.

A classic ABC used in quantum mechanics is the negative imaginary potential (NIP) method,[10] which applies a negative imaginary potential in a region near the cell boundaries. For example, inside a sphere of radius R the imaginary potential is zero, and outside the sphere, the potential changes

linearly from zero to negative imaginary infinity

$$V_{NIP}(r) = \begin{cases} 0, & \text{if } r \leq R \\ -i\alpha|r - R|, & \text{if } r > R. \end{cases} \quad (22)$$

Another approach is the mask function approach,[12] in which wave functions are multiplied by a mask function. The value of the mask function is unity inside the sphere and decays smoothly to zero outside the sphere. This is in practice, the same method as NIP, but operates directly on wave functions instead of the influence through the potential.

The perfectly matched layers method[13] is a widely used ABC, for example, in simulations of electromagnetic scattering. The basic idea is to tune the absorbing boundary dynamically based on the properties of outgoing waves. As waves can be absorbed without significant reflections in a distance which is proportional to their wavelength, waves with high momenta (i.e., those with small wavelengths), are absorbed stronger than waves with low momenta. In PML, this is done by modifying the kinetic energy operator as

$$\frac{-1}{2}\frac{\partial^2}{\partial^2 x} \rightarrow \frac{-1}{2}\frac{1}{1+i\gamma(x)}\frac{\partial}{\partial x}\frac{1}{1+i\gamma(x)}\frac{\partial}{\partial x}, \quad (23)$$

within the boundary layers. Above, $\gamma(x)$ is a parametrization function determining the strength of the absorption.

The direct use of the PML method would lead to an advection term. In general, advection terms have tendency to reduce stability and convergence of the propagation. Moreover, the advection term would break the (complex) symmetry of the SICN propagator. Therefore, we apply a simplified version of the PML method. We add an imaginary part to our kinetic energy

$$\langle \nabla\chi_i|\frac{1}{2}|\nabla\chi_j\rangle \rightarrow \langle \nabla\chi_i|\frac{1}{2} + i\sigma(\mathbf{r})|\nabla\chi_j\rangle, \quad (24)$$

where $\sigma(\mathbf{r})$ is a parametrization function decreasing from zero towards negative infinity. We call this approach negative imaginary kinetic energy (NIK) method, which can be seen as dynamic NIP where the strength of the imaginary potential depends on the kinetic energy of the outgoing wave. It could be also seen as a simplified version of the external complex scaling method.[44,45] This approach leads to complex symmetric matrices which allows complex symmetric conjugate gradient (CSCG) to be used with the SICN propagator. It is also clear how to implement a stable propagation scheme with NIK-ABC. This is discussed in Subsection III B 1. This is not the case for PML, as it changes the real part of the kinetic energy operator in addition to the imaginary part and it includes the complex advection term.

1. Stable propagation with absorbing boundaries

When the NIP or NIK method is applied with TP-TDDFT, the stability and qualitative behavior of the propagator must be investigated as the propagation is not unitary. For example, if NIP or NIK Hamiltonian is applied to both sides (left hand side (LHS) and right-hand-side (RHS)) of the SICN propagation equation, the propagation becomes unstable and its qualitative behavior is wrong when the imaginary component of the Hamiltonian is large. For small imaginary components, the polynomial expansion is accurate, the propagation is stable, and its qualitative behavior is correct, i.e., the norm of wave functions decreases. However, when the imaginary component is large, the norm does not decrease. Moreover, the sign of the wave function changes on each iteration. The simplified form

$$\frac{1 - i(a - ib)}{1 + i(a - ib)} = \frac{-b^2 - a^2 - 2ia + 1}{b^2 + 2b + a^2 + 1}, \quad (25)$$

based on Eqs. (14), (21) and (23) demonstrates the issue. When $b \rightarrow \infty$, this ratio approaches -1 as $\mathcal{O}(b^{-1})$. We have found this effect to cause numerical instabilities also in practice.

To restore the correct qualitative behavior, we apply the ABC Hamiltonian H_{ABC} only to the implicit part of the propagation equation (i.e., to the LHS of Eq. (15)):

$$\left\{S(t + \Delta t/2) + \frac{i}{2}\Delta t\left[H(t + \Delta t/2) + H_{\text{ABC}}\right]\right\} C(t + \Delta t)$$
$$= \left\{S(t + \Delta t/2) - \frac{i}{2}\Delta t\hat{H}(t + \Delta t/2)\right\} C(t). \quad (26)$$

In principle, the propagation is missing one half of the absorbtion, but the parametrization function $\sigma(\mathbf{r})$ can be multiplied by factor of two to approximately compensate the missing one half. If we use the same simplified notation (form) as before, we get

$$\lim_{b\rightarrow\infty} \frac{1 - ia}{1 + i(a - ib)} = b^{-1} + \mathcal{O}(b^{-2}). \quad (27)$$

And we see that the norm decreases always as b increases, i.e., the correct qualitative behavior is restored. With this modification, the above-mentioned numerical instability is removed also in practice.

C. Implementation

Our original FE-DFT implementation was based on the ELMER finite-element library.[46] However, for further development we chose to replace it by a more specialized code. Our implementation consists of three different parts: (i) a parallel sparse linear algebra library, (ii) a parallel FE library, and (iii) a (TD)DFT code which we have built on top of the first two ingredients. The parallel sparse linear algebra library is mostly a wrapper library based on Trilinos library developed in the Sandia National Laboratory.[43] The FE library completed in the present work employs hierarchical p-type tetrahedral elements. For parallelization, it uses a domain decomposition method.[47] In addition to the domain decomposition, TP-TDDFT is parallelized over KS states.

IV. PERFORMANCE

We apply our implementation to a set of systems within the linear response regime, namely, to the sodium dimer Na_2, benzene C_6H_6, and fullerene C_{60} molecules. For Na_2, we calculate semi-core excitations in addition to valence excitations. Furthermore, we apply an intense laser pulse to the Mg atom in order to test within the nonlinear regime. Finally, we probe

valence electrons of the Mg atom by semi-core excitations before and after an intense laser pulse.

In all simulations, we use the polynomial degree $p = 2$, ALDA exchange-correlation function, and NIK absorbing boundary conditions with

$$\sigma(\mathbf{r}) = \begin{cases} -\gamma |r_{\min}(\mathbf{r}) - R_{cut}|^2, & \text{if } r_{min}(\mathbf{r}) > R_{cut} \\ 0, & \text{otherwise,} \end{cases} \quad (28)$$

where $r_{\min}(\mathbf{r})$ is the distance to the closest atom nucleus. The parameter R_{cut} was chosen to be $5.0a_0 \approx 2.6$ Å and $\gamma = 0.01a_0^{-2}$. The R_{cut} might seem as a short distance, but a small γ makes ABC very weak in the vicinity of nuclei. These parameters were found to be a good compromise in order to prevent artificial reflections while not disturbing electron dynamics.

To demonstrate the difference between NIK and NIP absorbing boundary conditions (Eqs. (22) and (24), respectively), we show their effect on the photoabsorption spectrum of a hydrogen atom in Fig. 1. The NIK is more efficient in absorbing high energy waves as the strength of the absorption increases with the momentum. This is clearly demonstrated in the case of weak absorbing boundaries, where artificial peaks at higher energies smooth out much more efficiently for NIK than NIP. Moreover, if we increase the strength of the absorption, the NIP begins to shift the low end of the spectrum to higher energies, whereas the NIK has no apparent shift. The NIK is especially useful for our FE method as high frequency waves are absorbed soon after they propagate away from nuclei, which allows us to reduce degrees of freedom as the distance from nuclei increases.

The preconditioner was used in all calculations with the shift $\alpha = 1.0$ hartree. In general, without a preconditioner, the CSCG iteration will fail to converge within 1000 iterations, whereas with the preconditioner, CSCG will take around 100 iterations depending somewhat on the system. Fine tuning α can slightly reduce the number of CSCG iterations required. To further emphasize the importance of the preconditioning, we remark that even such a simple system as a hydrogen atom does not converge without preconditioning, whereas with preconditioning it converges on average with 55 iterations per time-step. If we loosen the convergence criterion several orders of magnitude and use a reduced mesh which leads to a better conditioning number (but to unconverged results), the unpreconditioned propagation converges on average with 420 iterations per time-step, whereas the preconditioned propagation converges with only eight iterations. Clearly, preconditioning is necessary in any practical simulation.

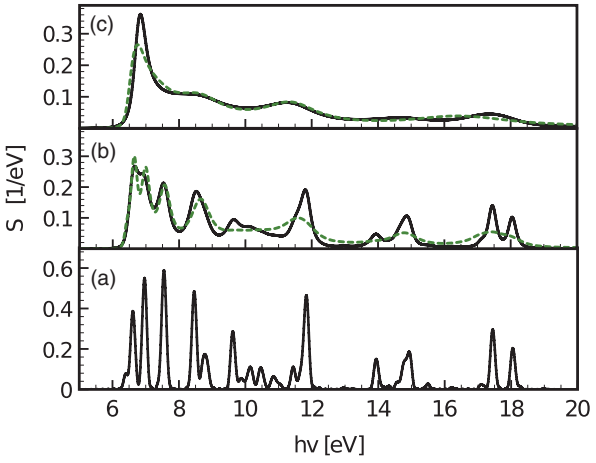

FIG. 1. Optical absorption spectra of a hydrogen atom with different boundary conditions: (a) without absorbing boundary condition, (b) with weak NIP (solid) and NIK (dashed) absorbing boundaries, and (c) with strong absorbing boundaries.

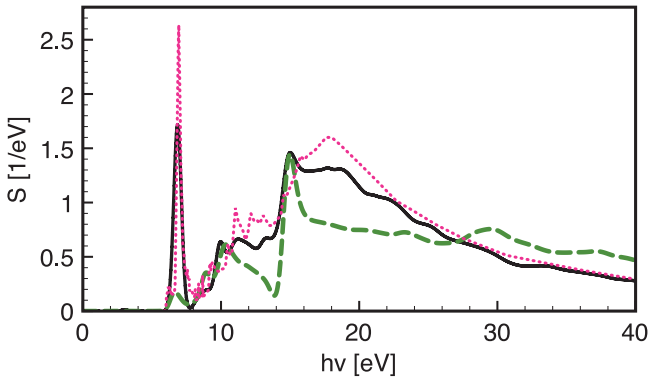

FIG. 2. Optical absorption spectrum of C_6H_6 calculated using the FE-TP-TDDFT (solid line), its out-of-molecular-plane component (dashed line), and the experimental spectrum (dotted line).

A. Valence excitations

Figure 2 shows the optical absorption spectrum of C_6H_6 calculated using our FE method. C_6H_6 has a planar geometry with the C–C bond length of 1.396 Å and the C–H bond length of 1.083 Å. The total simulation time is 24 fs, time-step 8 as, and only valence states are propagated. ALDA is know to perform well in this case and the experimental spectrum[48] is in excellent agreement with the calculated spectrum. The essential features are seen clearly, for example, the first peak at ~7 eV. Yet, the continuum of the spectrum is smooth without artificial peaks, which indicates that our NIK-ABC method is working properly.

A computationally more challenging test for the method and the code is C_{60}. Figure 3 shows a comparison of our FE

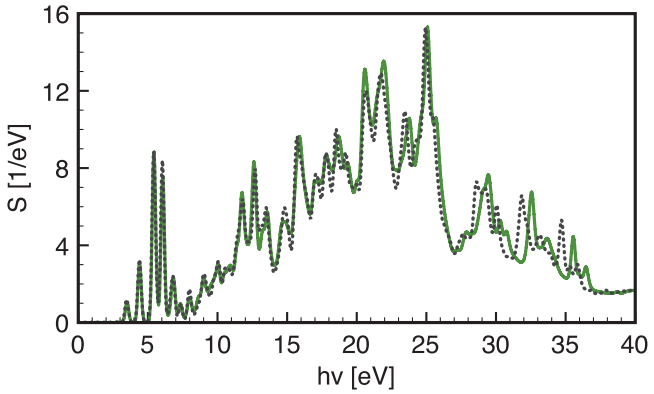

FIG. 3. Optical absorption spectra of C_{60} calculated using the FE-TP-TDDFT (solid line) and FD-PAW-TP-TDDFT (dotted line) methods.

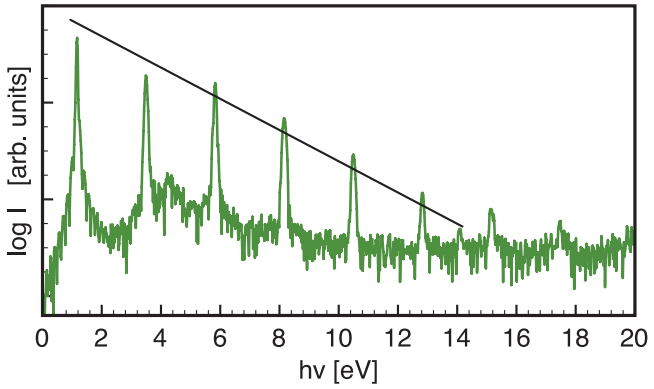

FIG. 4. Emission spectrum of the Mg atom when hit by an long, intense NIR laser pulse (178 fs, 1064 nm ↔ 1.165 eV). The solid straight line corresponds to an exponential decay.

method with the FD-PAW method calculated using the GPAW program package.[16,49] Both spectra are calculated with the time step of 8 as. The diameter of C_{60} is 7.1 Å. The low energy parts of the spectra are practically identical. The peak positions begin to differ slightly above 30 eV but the spectra have still the same structure. This is a remarkable agreement between two different methods and implementations.

To simulate an intense CW laser field, we apply a long (178 fs) NIR ($\lambda = 1064$ nm $\leftrightarrow$ $\omega = 1.165$ eV) laser pulse to the Mg atom. The nonlinear response of the atom creates odd integer multiples of the laser frequency, called harmonics. Their intensity should decay exponentially, unless the frequency of a harmonic is close to a resonant transition frequency. Near a resonance the harmonic is enhanced. This can also be seen in Fig. 4 in the emission spectrum for the Mg atom. The intensity decays exponentially except for the 5th harmonic near 6 eV, which is slightly enhanced because of nearby resonances (the shoulder of the main peak, similar to what is seen in Fig. 5 for a sodium atom.)

B. Core excitations

As the above examples show, our method performs extremely well for valence states. Next, we demonstrate our method for semi-core states of the Na atom and the sodium dimer Na_2. The absorbtion spectra of the Na and Na_2 are shown in Fig. 5. In addition to the 3*s* state of Na, we include the 2*s* and 2*p* semi-core states to the calculation. For Na_2, we include the $2\sigma_g$, $2\sigma_u$, $3\sigma_g$, $1\pi_u$, $1\pi_g$, $3\sigma_u$, and $4\sigma_g$ states. The $4\sigma_g$ state is the HOMO valence state and the rest are semi-core states. The atomic and dimer semi-core states are almost degenerate, but a change in the chemical environment changes the semi-core absorption spectrum in addition to the valence absorption spectrum. As can be seen from Fig. 5, this is captured by our method.

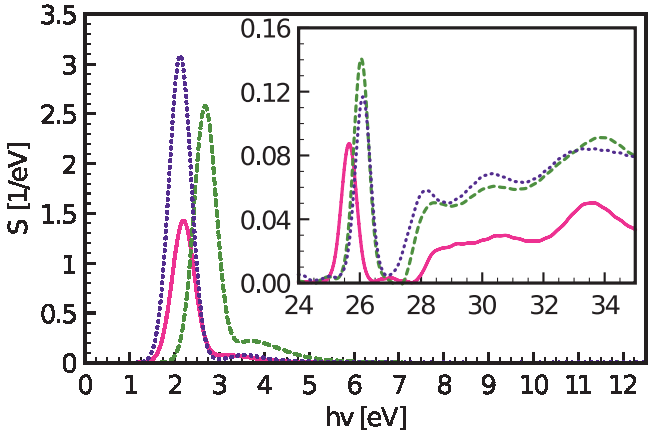

FIG. 5. Optical absorption spectra of Na (solid line) and Na_2 calculated with FE-TP-TDDFT. For the dimer, components perpendicular (dashed line) and parallel (dotted line) to the molecular axis have been separated.

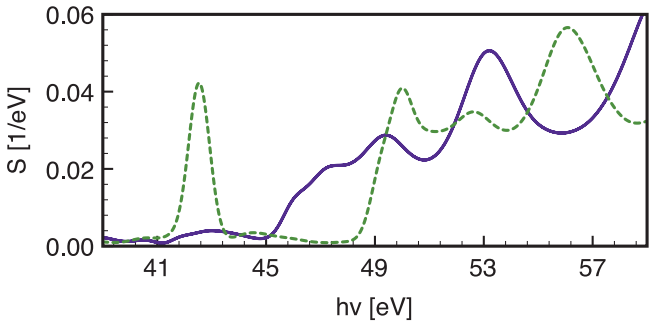

FIG. 6. Semi-core absorption spectrum of the Mg atom before (solid line) and after (dashed line) a short, intense NIR laser pulse (3.6 fs, 1064 nm).

Unfortunately, ALDA does not perform well for semi-core and core electrons, mainly due to self-interaction of electrons on localized states. For example, the first semi-core peak of the sodium atom is approximately 5 eV below the experimental value.[50] Several approximations for the exchange-correlation functional have been proposed, which address the self-interaction. Probably the simplest self-interaction correction was proposed by Perdew and Zunger,[51] but most likely more appropriate for our purposes would be the time-dependent KLI approximation of the exact exchange.[52] Even though the self-interaction error has to be addressed in simulations of real systems, it is a deficiency of the model, not that of our discretization method. For this reason, it is not in the scope of this work, but will be addressed in future.

As the final test, we simulate the semi-core spectrum of the Mg atom before and after a short, intense NIR laser pulse (3.6 fs, 1064 nm). Figure 6 shows how the laser pulse creates a hole to the 3*s* valence state and a new excitation from the 2*p* state to the 3*s* state becomes allowed. Moreover, other excitations from the 2*p* state move now to higher energies. Again, we have the self-interaction problem and the semi-core excitations are at too low energies. Nevertheless, this test clearly demonstrates that our method is able to track changes in valence states by using semi-core excitations as probes.

V. CONCLUSIONS

We have presented an all-electron method for TDDFT using the time-propagation approach. The method employs highly nonuniform finite-element bases, which allow a full 3D all-electron discretization. We introduced a preconditioner for the propagation equation improving the conditioning of the equation and making the propagation viable in these bases. We also discussed how absorbing boundary conditions should

be implemented and we described a new boundary condition inspired by the perfectly matched layers method.

The method was verified to work within the linear response regime for valence states by comparing its results to a known experimental result (C_6H_6) and to those obtained by another code (GPAW). The semi-core excitations were shown to react to the chemical environment. The nonlinear response reproduced the expected behavior. The method was also able to probe nonlinear dynamics of valence states by using semi-core excitations as probes, i.e., simulating an experiment in which an atom undergoes successively valence and core electron excitations.

However, semi-core excitations were found to be several eVs too low, which is clearly unacceptable for simulations of real systems. The error arises mainly from the ALDA functional which suffers from a significant self-interaction error. The ALDA has also incorrect asymptotic behavior leading to significantly too low ionization thresholds. Therefore, we will implement more advanced XC functionals in near future. Moreover, we will examine how to efficiently simulate deeper core states. Especially, how the difference in time-scales of deep core states and valence states can be addressed without a significant increase in the computational effort.

Nevertheless, our code can handle hundreds of electrons, it works on the linear and nonlinear regimes, and in addition to valence states, it can handle dynamics of semi-core electrons. The required degrees of freedom for FE discretization do not depend significantly on states of interest, in contrast to, for example, finite-difference or planewave discretizations, where semi-core states of sodium atom require ten times larger planewave cutoff than valence states (i.e., over 30 times more DOFs).[53] Moreover, our systematically improvable all-electron basis is excellent benchmarking, for example, exchange-correlation functionals, and pseudo-potentials.

ACKNOWLEDGMENTS

This work was performed in COMP which is the Center of Excellence, Academy of Finland. The calculations were performed using resources of CSC-IT Center for Science Ltd. and Aalto University's Triton cluster. L.L. acknowledges support from the French ANR (ANR-08-CEXC8-008-01).

[1] F. Krausz and M. Ivanov, Rev. Mod. Phys. **81**, 163 (2009).
[2] E. Goulielmakis, Z.-H. Loh, A. Wirth, R. Santra, N. Rohringer, V. S. Yakovlev, S. Zherebtsov, T. Pfeifer, A. M. Azzeer, M. F. Kling, S. R. Leone, and F. Krausz, Nature **466**, 739 (2010).
[3] W. Kohn, Rev. Mod. Phys. **71**, 1253 (1999).
[4] E. Runge and E. Gross, Phys. Rev. Lett. **52**, 997 (1984).
[5] K. Yabana and G. F. Bertsch, Phys. Rev. B **54**, 4484 (1996).
[6] M. Marques and A. Rubio, in *Time-Dependent Density Functional Theory*, Lecture notes in Physics, Vol. 706 (Springer-Verlag, Berlin, Heidelberg, 2006), Chap. 15, pp. 225–240.
[7] J. Krueger and N. T. Maitra, Phys. Chem. Chem. Phys. **11**, 4655 (2009).
[8] M. Thiele and S. Kümmel, Phys. Rev. A **79**, 052503 (2009).
[9] C. Ullrich and A. Bandrauk, in *Time-Dependent Density Functional Theory*, Lecture notes in Physics, Vol. 706 (Springer-Verlag, Berlin, Heidelberg, 2006), Chap. 24, pp. 357–375.
[10] D. Neuhasuer and M. Baer, J. Chem. Phys. **90**, 4351 (1989).
[11] T. Nakatsukasa and K. Yabana, J. Chem. Phys. **114**, 2550 (2001).
[12] M. A.L. Marques, A. Castro, G. F. Bertsch, and A. Rubio, Comput. Phys. Commun. **151**, 60 (2003).
[13] J. Berenger, J. Comput. Phys. **114**, 185 (1994).
[14] C. Zheng, J. Comput. Phys. **227**, 537 (2007).
[15] O. Sugino and Y. Miyamoto, Phys. Rev. B **59**, 2579 (1999).
[16] M. Walter, H. Häkkinen, L. Lehtovaara, M. Puska, J. Enkovaara, C. Rostgaard, and J. J. Mortensen, J. Chem. Phys. **128**, 244101 (2008).
[17] S. Meng and E. Kaxiras, J. Chem. Phys. **129**, 054110 (2008).
[18] M. C. Payne, M. P. Teter, D. C. Allan, T. A. Arias, and J. D. Joannopoulos, Rev. Mod. Phys. **64**, 1045 (1992).
[19] P. E. Blöchl, Phys. Rev. B **50**, 17953 (1994).
[20] M. J. Turner, R. W. Clough, H. C. Martin, and L. J. Topp, J. Aeronaut. Sci. **23**, 805 (1956).
[21] B. Szabo and I. Babuska, *Finite Element Analysis* (Wiley Interscience, New York, 1991).
[22] L. Lehtovaara, V. Havu, and M. Puska, J. Chem. Phys. **131**, 054103 (2009).
[23] H. Yu, A. Bandrauk, and V. Sonnad, J. Math. Chem. **15**, 273 (1994).
[24] H. Yu and A. D. Bandrauk, J. Chem. Phys. **102**, 1257 (1994).
[25] B. I. Schneider, L. A. Collins, and S. X. Hu, Phys. Rev. E **73**, 036708 (2006).
[26] M. S. Pindzola, G. J. Bottrell, and C. Bottcher, J. Opt. Soc. Am. B **7**, 659 (1990).
[27] G. Vignale, Phys. Rev. A **77**, 062511 (2008).
[28] A. D. Bandrauk, S. Chelkowski, D. J. Diestler, J. Manz, and K.-J. Yuan, Phys. Rev. A **79**, 023403 (2009).
[29] D. B. Milosevic, G. G. Paulus, D. Bauer, and W. Becker, Journal of Physics B **39**, R203 (2006).
[30] E. K. U. Gross and W. Kohn, Phys. Rev. Lett. **55**, 2850 (1985).
[31] M. Bern and D. Eppstein, in *Computing in Euclidean Geometry*, 2nd ed., edited by D.-Z. Du and F. Hwang (World Scientific, Singapore, 1995), pp. 47–123.
[32] J. R. Shewchuk, "Delaunay refinement mesh generation," Ph.D. dissertation (School of Computer Science, Carnegie Mellon University, Pittsburgh, Pennsylvania, 1997) (available as Technical Report CMU-CS-97-137).
[33] C. Schwab, *p- and hp-finite element methods* (The Clarendon Press, Oxford University Press, New York, 1998).
[34] A. Castro, M. A. L. Marques, and A. Rubio, J. Chem. Phys. **121**, 3425 (2004).
[35] E. Hairer, C. Lubich, and G. Wanner, *Geometric Numerical Integration: Structure-Preserving Algorithms for Ordinary Differential Equations* (Springer, New York, 2006).
[36] X. Qian, J. Li, X. Lin, and S. Yip, Phys. Rev. B **73**, 035408 (2006).
[37] K. Yabana and G. F. Bertsch, Phys. Rev. A **60**, 1271 (1999).
[38] T. Brabec and F. Krausz, Rev. Mod. Phys. **72**, 545 (2000).
[39] M. Protopapas, C. Keitel, and P. Knight, Rep. Prog. Phys. **60**, 389 (1997).
[40] A. Brandt, S. McCormick, and J. Ruge, in *Sparsity and Its Applications* (Cambridge University Press, Cambridge, 1985), pp. 257–284.
[41] P. V. Ek, J. Mandel, and M. Brezina, Computing **56**, 179 (1996).
[42] M. Gee, C. Siefert, J. Hu, R. Tuminaro, and M. Sala, ML 5.0 Smoothed Aggregation User's Guide, Technical Report SAND2006-2649 (Sandia National Laboratories, Albuquerque, NM, 2006).
[43] M. A. Heroux, R. A. Bartlett, V. E. Howle, R. J. Hoekstra, J. J. Hu, T. G. Kolda, R. B. Lehoucq, K. R. Long, R. P. Pawlowski, E. T. Phipps, A. G. Salinger, H. K. Thornquist, R. S. Tuminaro, J. M. Willenbring, A. Williams, and K. S. Stanley, ACM Trans. Math. Softw. **31**, 397 (2005).
[44] W. P. Reinhardt, Annu. Rev. Phys. Chem. **33**, 223 (1982).
[45] F. He, C. Ruiz, and A. Becker, Phys. Rev. A **75**, 053407 (2007).
[46] See http://www.csc.fi/english/pages/elmer for CSC - IT Center for Science (CSC): Elmer, open source finite element software for multiphysical problems.
[47] G. Karypis and V. Kumar, SIAM J. Sci. Comput. (USA) **20**, 359 (1998).
[48] E. E. Koch and A. Otto, Chem. Phys. Lett. **12**, 476 (1972).
[49] J. Enkovaara, C. Rostgaard, J. J. Mortensen, J. Chen, M. Dulak, L. Ferrighi, J. Gavnholt, C. Glinsvad, V. Haikola, H. A. Hansen, H. H. Kristoffersen, M. Kuisma, A. H. Larsen, L. Lehtovaara, M. Ljungberg, O. Lopez-Acevedo, P. G. Moses, J. Ojanen, T. Olsen, V. Petzold, N. A. Romero, J. Stausholm-Møller, M. Strange, G. A. Tritsaris, M. Vanin, M. Walter, B. Hammer, H. Häkkinen, G. K.H. Madsen, R. M. Nieminen, J. K. Nørskov, M. Puska, T. T. Rantala, J. Schiøtz, K. S. Thygesen, and K. W. Jacobsen, J. Phys.: Condens. Matter **22**, 253202 (2010).
[50] *Advances in Research and Applications*, Solid State Physics, Vol. 29, edited by H. Ehrenreich, F. Seitz, and D. Tumbull, (Academic, New York, 1974), p. 53.
[51] J. P. Perdew and A. Zunger, Phys. Rev. B **23**, 5048 (1981).
[52] C. A. Ullrich, U. J. Gossmann, and E. K. U. Gross, Phys. Rev. Lett. **74**, 872 (1995).
[53] M. Gatti, I. V. Tokatly, and A. Rubio, Phys. Rev. Lett. **104**, 216404 (2010).